Progress in Biomaterials (2022) 11:79–94
https://doi.org/10.1007/s40204-022-00181-y

ORIGINAL RESEARCH

Drug infused Al_2O_3-bioactive glass coatings toward the cure of orthopedic infection

P. Bargavi[1] · R. Riju Chandran[1] · D. Durgalakshmi[2] · P. Rajashree[4] · R. Ramya[3] · S. Balakumar[1]

Received: 25 September 2021 / Accepted: 11 January 2022 / Published online: 30 January 2022
© The Author(s), under exclusive licence to Islamic Azad University 2022

Abstract

A unique implant coated substrate with dual-drug-eluting system exhibiting antibacterial, anti-inflammatory, and bone regenerative capacity has been fabricated using spray pyrolysis deposition (SPD) method. Bioglass (BG) and BG-alumina (BG-Al) composites coatings with different concentrations of Al incorporated on BG network over the Cp-Ti substrate were fabricated using SPD technique. Phase purity of BG and BG-Al composites were analyzed by XRD in which $Na_2Ca_2Si_3O_9$ and β-$Na_2Ca_4(PO_4)_2SiO_4$) and $Na_{7.15}(Al_{7.2}Si_{8.8}O_{32})$ phases were formed. Surface morphology of the coated substrates was analyzed by SEM. Uniformity of the coatings were evaluated by surface profilometer and the uniform distribution the nanoparticles were confirmed with Elemental mapping. Systematically, each apatite layer formation on coated substrate was confirmed by immersing the samples for 1, 3, and 7 days in simulated body fluid and the needle-like structure was characterized using SEM. Cumulative release of Tetracycline hydrochloride (Tet) antibiotic and Dexamethasone (Dex) anti-inflammatory drug-loaded BG-Al and BG-Al composite-coated substrate were studied for 24 h. Antibacterial activity of the coated substrates were evaluated by time-dependent growth inhibition and minimal inhibitory concentration (MIC) assays in which BG-Al and BG-Al composite loaded with Tet showed considerable growth inhibition against *S. aureus*. Osteoblast-like cells (MG-63) exhibited profound proliferation with no cytotoxic effects which was due to release of Dex drug-coated substrates. Thus, surface modification of Cp-Ti substrate with BG, BG-Al composites coatings loaded with Tet and Dex drug can be considered for post-operative orthopedic implant infection application.

Keywords Bioglass · Spray pyrolysis · Antibiotic · Anti-inflammatory · Orthopedic infection

Introduction

Today, most countries in the world are having high elderly population, and due to presence of comorbidity such as osteoporosis, diabetes, and bone tumors, there is a growing demand for efficient implant material. Bacterial infection is one of the most frequent problems related to implant surgery (Guilherme et al. 2006). Formation of bacterial biofilms due to settlement and proliferation of bacteria on surface of implantable devices results in many serious problems such as delaying healing process, causing implant failure (Wheeler and Stokes 1997). Colonization of bacteria on implant surface triggers inflammation in the adjacent tissues leading to bone degradation. Furthermore, sustained immune response to the implant-associated biofilm often leads to a state of chronic inflammation, which complicates post-op treatments (Gil-Albarova et al. 2004). In spite of fragmentary medical advances in refining the choice of materials or surgeries, considerable risk of implants becoming infected still lingers (Niedzielski et al. 2011). In addition to microbes being introduced during the time of surgery, there is a constant challenge from bacteria in the systemic circulation that tends to aggregate on vulnerable implant surface. Prevalence of implant infection ranges from 2.5% in hip and knee replacement surgery to 10% in joint revision surgeries (Hench et al. 1998). Contaminated implants pose an onerous clinical task.

✉ S. Balakumar
balasuga@yahoo.com

1 National Centre for Nanoscience and Nanotechnology, University of Madras, Guindy Campus, Chennai 600 025, India

2 Department of Medical Physics, Anna University, Chennai 600 025, India

3 Saveetha Dental College & Hospitals, SIMTS, Poonamallee High Road, Chennai 600089, India

4 CAS in Crystallography & Biophysics, University of Madras, Guindy campus, Chennai 600 025, India

Characteristically, despite prolonged antibiotic therapy, once infected, implants require surgical removal. This increases patient morbidity and economic burden (Felora and Reza 2011). Antibiotics are still unsurpassable in preventive management of implant infections. Conversely, the antimicrobial potency of antibiotics is deteriorating over time due to the development of resistant microbial strains.

As a consequence, the risk of implant infection is increasing provoking researchers to explore novel ways to counteract such infections. Most of the bacterial species have been reported to be found attached in surface-related biofilms, rather than detached forms (Francesco and Enrica 2017). Irrevocable adherence to the implant surface occurs with adhesion proteins contributing to 80% of clinical microbial infections. Rendering the implant surface less vulnerable to bacterial colonization would vividly lower the rate of infection (Ghannam et al. 2001). Implant surface modification can be effectively accomplished by coating with bioactive glass (BG). BG is an exemplary material made of silica, calcium, and boron, which possesses inherent biocompatibility (Manam et al. 2017).

BG has an innate potential of high strength, low weight, and has wide spectra of biomedical applications, specifically in areas related to tissue regeneration and restorative dentistry (Laczka et al. 2000). Among the various types of BG, borate BG has demonstrated potent antimicrobial property even with highly pathogenic strains of MRSA and *E. coli*. Improved antimicrobial property is attained with increased pH of the tissue microenvironment that is a deterrent to bacterial growth and prevents biofilm formation on the BG surface (Clark 2010).

Antimicrobial efficacy of BG has been well established in in vitro studies against staphylococcus and streptococcus strains. Ability of BG to produce hostile environment to bacterial growth than a direct contact killing mode makes it a more persuasive antimicrobial agent against most of the bacterial strains (Dalal et al. 2012). Furthermore, such antibacterial mechanism does not allow bacteria to develop resistance to the antimicrobial effects of BG (Wang 2003). Bacterial challenges during implant placement are usually handled by administering prophylactic antibiotics before surgical procedure; however, its use is highly debatable as inadvertent antibiotic use leads to development of resistant strains (Wu et al. 2007a). Antibiotic drug delivery is done systemically or locally, while local application is considerably advantageous due to lesser cost, low systemic toxicity, and increased concentration at the site of therapy (Verrier et al. 2004). Alteration of the implant surface by coating and other modifications offers a highly promising potential in preventing implant failure. Coating the surface of implants with antimicrobial agents is advantageous than systemic intake due to increased drug availability (Pamuła et al. 2012).

Implant surface modification with BG coating on Cp-Ti implants has been translated to clinical use in orthopedics and dentistry exhibiting successful outcomes in terms of longevity (Ashok et al. 2018; Mosab and Han-Chole 2021a; Tehseen et al. 2021). BG coating exhibits enhanced biocompatibility response with no adverse effects with minimal inflammation in the implant tissue interface. Moreover, BG coating results in improved cell attachment and augmented mineralization of the extracellular matrix. Besides, BG-coated implant bone interface shows significantly higher osseointegration than the conventional implants (Durgalakshmi et al. 2018; Mosab and Han-Chole 2021b).

Recently, mesoporous BG has been the focus for many bio-material research groups owing to its novel properties such as resorbability, osseoconductivity, and renewal of bone-like structure. These qualities make mesoporous BG, an ideal substance for bone grafting and bone regeneration therapy (Tehseen et al. 2021). Nevertheless, BG has certain disadvantages as implant surface modifier due to low fracture strength, toughness, and relatively high solubility (Durgalakshmi et al. 2018).

This challenge was addressed by a process of combining BG to materials with more stable crystalline structure such as alumina (Al). Al is basically a bioinert ceramic with excellent biocompatible properties (Mosab and Han-Chole 2021b). Mechanical properties of Al are superior when compared with BG (Mahwish et al. 2015). Hence, incorporation of Al with a bio-material has proven to produce enhanced mechanical properties without reduction in biocompatibility (Indranee et al. 2016). Additionally, their mesoporous structure gives them special surface features (Pamula et al. 2011) and converts them into suitable form for drug delivery of certain substances.

The aim of this study is to develop nanocoatings with antibacterial and biocompatible properties for orthopedic implants by means of spray pyrolysis method. Alumina-incorporated bioglass (Al-BG) was chosen as an implant coating as it is biocompatible with controlled ion release properties. Al-BG has demonstrated properties to be considered as an effective drug-delivery system in other dental and orthopedic applications (Durgalakshmi et al. 2015). Hence, two drugs Tetracycline (Tet) and Dexamethasone (Dex) were loaded to Al-BG. Tetracycline (Tet) is a broad-spectrum antibiotic that has pronounced bacterial inhibiting property. It is specifically effective against peri-implantitis caused by pathogens like staphylococci and coliforms (Kokubo and Takadama 2006a), while Dexamethasone (Dex) is a potent anti-inflammatory drug. Developed implant coatings were subjected to a series of physicochemical analysis that included drug content and release profile, particle configuration, variability in simulated physiological conditions, and surface roughness. Besides, antibacterial activity and in vitro biocompatibility were evaluated with *S. aureus*, *B. subtilis*,

E. coli, and *P. aeruginosa* and human osteoblast like cell line—MG-63, respectively.

Materials and methods

Materials

Titanium foil, 1.0 mm(0.040 in) thick, 99.2% (metal basis)—commercially pure titanium grade II (Cp-Ti) substrate—(Alfa Aesar), tetraethyl ortho silicate (TEOS)-(Alfa Aesar), calcium nitrate ($CaNO_3$)-(Spectrum), orthophosphoric acid (H_3PO_4)-(Fisher Scientific), sodium hydroxide pellets (NaOH)-(Merck), sodium chloride (NaCl)-Merck, potassium chloride (KCl)-SRL, sodium dihydrogen phosphate (NaH_2PO_4)-RANKEM laboratory, potassium dihydrogen phosphate (KH_2PO_4)-Merck,. Hanks balanced salt solution (HBSS)-Sigma Aldrich, Dulbecco's minimal essential medium (DMEM)-(HiMedia), fetal bovine serum (FBS)—(HiMedia), antibiotic and antimycotic solution-(Sigma), phosphate buffer solution, ethanol, acetone (SRL). MG-63 osteoblasts like cells were obtained from NCCS Pune, India. Cells were cultured and maintained at 37 ºC with 5% CO_2.

Methods

Preparation of BG-Al coating on Cp-Ti substrate

The Cp-Ti titanium substrate was polished with silica carbide grit sheets and treated with acetone ultrasonication for a period of 30 min for a thorough cleansing process. Surface etching of Cp-Ti substrates was carried out by immersing the plate in hydrofluoric acid (HF) for 10 s and further washed with distilled water. Pre-heating of the substrates was carried out at 500 ºC in a hot plate integrated in spray pyrolysis unit. Bioactive glass (BG) with a composition (% by wt) of 45% SiO_2:24.5% Na_2O:24.5% CaO:6% P_2O_5 was chosen for our study (Kohal et al. 2011).

Sol preparation of 45S5 BG was done with SiO_2, CaO, P_2O_5, and Na_2O derived from tetra ethyl orthosilicate (TEOS), calcium nitrate ($CaNO_3$), orthophosphoric acid, and sodium hydroxide (NaOH). Alumina was incorporated by adding 5, 10, and 15 (% by wt) of aluminum chloride as an alumina source in BG sol. Ethylene glycol (5%) was used as a binder; it was added and stirred well for 2 h. The prepared of BG sol and alumina-added BG sol was spray coated over Cp-Ti substrates (cut into pieces of 2 cm × 1 cm) with spray pyrolysis technique. Densification of coatings was achieved by sintering, which involved heating and cooling rate of 10 °C/min by 800 °C for 3 h. The obtained samples were referred to as BG and BG-Al, respectively.

Materials and coatings' characterizations

The degree of crystallinity was assessed by Gracing Incidence X-ray powder diffraction GI-XRD (PANalytical Instruments, The Netherlands) operating at a voltage 40 kV and current of 25 mA with $CuK_{\alpha 1}$ as X-ray radiation source. Scanning was done at 2θ range of 20°–50°. Peaks were assigned and correlated with Joint Committee on Powder Diffraction Standards (JCPDS). Morphological configurations of nanobiocomposites were analyzed with SEM (Hitachi SU-6600, Japan). Elemental analysis was performed using EDS (Horiba 8121-H, Japan).

In vitro biomineralization assay

Simulated body fluid (SBF) was prepared as described by Kokubo and coworkers (Raja et al. 2016). Bioactivity was investigated by immersion in SBF for 1, 3, and 7 days at baseline temperature of 37 °C. After removal from SBF, films were rinsed using double-distilled (DD) water and dried. Apatite layer deposition before and after immersion was assessed with SEM micrographs.

Hemocompatibility assay

Hemocompatibility assay was performed with 5 mL of blood collected by venipuncture from healthy volunteers. Ethylene diamine tetra acetic acid was added to the collected blood to prevent coagulation. Centrifugation was done at 4000 rpm for 10 min at 4 °C. Erythrocytes (RBCs) after centrifugation were rinsed and suspended in PBS (pH 7.4). Pure BG and BG-Al-coated Cp-Ti substrates were added with 950 µL of PBS in a 6-well plate containing 50 µL RBCs in PBS that was incubated at 37 °C for 1 h in a shaker. Subsequently, sample transfers were done in 1 mL centrifuge vials and were again centrifuged at 4000 rpm for 10 min at 4 °C and supernatants were obtained. Absorbance was measured at 540 nm using UV–Vis spectrophotometer (Geetha et al. 2009). Percentage of hemolysis was calculated with Eq. (1)

$$\text{Hemolytic percentage} = \frac{\text{sample absorbance} - \text{negative control}}{\text{positive control} - \text{negative control}} \times 100. \quad (1)$$

Cell culture and Cell proliferation assay

Cell proliferation assay was conducted with human osteoblast-like MG-63 cell lines, (NCCS, Pune, India). Cell seeding was done onto 6-well plates. Dulbecco's Modified Eagle's Medium (DMEM) supplemented with 10% fetal bovine serum (FBS) and 1% antibiotic/antimycotic solution was used as culture medium. Plates were incubated in 5% CO_2 at 37 °C till the cells attained 70% confluence.

Thin-film samples were placed in the cultured well plates and observed for 24 h, 48 h, and 72 h. Cell separation was realized with 0.25% trypsin EDTA and cells were seeded onto 96-well plates at a cell density of 5×10^4 cells per well for further proliferation assay. MTT (3-(4,5-dimethylthiazol-2-yl)-2,5-di-phenyltetrazolium bromide) assay was done to analyze cell proliferation. Sample transfer was done to 96-well plate, further addition of 30 µL of MTT reagent to each well was done and plates were subjected to incubation for 4 h at 37 °C. MTT was reduced to formazan by metabolically active cells. Formazan was dissolved with 300 µL of dimethylsulfoxide (DMSO) and absorbance measured at 570 nm in an ELISA reader (Inuzuka et al. 2004). Percentage of cell viability calculation was done using Eq. (2)

$$\text{Cell viability}(\%) = \frac{\text{OD of Treated}}{\text{OD of Control}} \times 100. \quad (2)$$

In vitro drug loading and releasing profile

Our main aim was to prepare the drug-loaded thin films and to analyze its efficiency on bacterial growth inhibition and cell proliferation. In this study, we have chosen two different drugs; Tetracycline hydrochloride (Tet)—an antibiotic; and Dexamethasone sodium phosphate (Dex)—an anti-inflammatory drug. BG and BG-Al composites act as nanocarriers. Dex (10 mg) and Tet (10 mg) were taken and dissolved in 15 mL of PBS solutions and added in a separate 6-well plate and the spray-coated BG and BG-Al-coated substrates were immersed overnight in the drug solution at 37 ºC with 50 rpm, and then removed and dried. Using the supernatant, the amount of drug loaded was calculated by dividing the amount of total drug loaded divided by the total weight of the substrates. Furthermore, the loading and releasing profiles of Tet- and Dex-loaded-coated substrates in PBS solution were evaluated using UV–Vis spectrophotometer at 362 nm and 300 nm as well, as shown in Eq. (3)

$$\left[\text{Drug loading content}\,(\%) = \frac{\text{Weight of the drugs loaded in coated substrates}}{\text{Weight of the coated substrates}} \times 100\right] \quad (3)$$

$$\left[\text{Drug releasing}\,(\%) = \frac{\text{Initial conc (drug)} - \text{Final conc (drug)}}{\text{Intial Conc (drug)}} \times 100\right] \quad (4)$$

Time-dependent growth inhibition assay

Assessment of bacterial growth was done from growth curve. Fresh colonies were inoculated on Muller Hinton Agar (MHA) and 50 mL of Luria–Bertaini (LB) medium. Optical density of 0.1 at 600 nm (O.D. of 0.1 corresponds to 10^8 CFU/mL of medium) was used as reference for growth limit. Further BG, BG-Al, BG-Al-T, LB alone, and only S. aureus as control were added with 2×10^8 CFU/mL. All the flasks were kept incubated at 37 °C with 50 rpm under shaking. Optical density measurement for every 0.5, 1, 2, 3, to 24 h time points at 600 nm was done to assess bacterial growth (Nayak et al. 2010).

Antibacterial activity

Bacterial species *B. subtilis*, *E. coli*, *S. aureus*, and *P. aeruginosa* strains were chosen and inoculated individually in 10 mL of Luria–Bertani (LB) media. As broth started becoming turbid, preparation of stock broth was done. Microbial loop was used to pick up the culture from the broth and was inoculated into the newly prepared sterile broth which was incubated at 37 °C. This condition was maintained till the growth peaked to the mid-log phase. Furthermore, to obtain a pellet of cells, broth was centrifuged at 4000 rpm for 15–20 min at 4 °C. Pellet was washed with PBS three times and suspended in 50 mL of PBS (Scheme 1).

BG-Al-coated Cp-Ti substrates containing BG, BG-Al 5%, BG-Al 10%, and BG-Al 15% were placed in sterile broth, to which the prepared cell suspension was added. This was further incubated for 6–8 h in an orbital shaker. Proportion of sterile water: broth: cell suspension amounted to 8:1:1. Serial dilutions of cells were done in sterile PBS and plated using a spread plate. Controls for the test sample were duly maintained. On further incubation for 8–12 h, cells and colony forming unit (CFU/mL) were counted and their profiles were produced (Xie et al. 2005).

Results and discussion

Crystal structure analysis

XRD patterns of BG and BG-Al coated Cp-Ti substrates are depicted as in Fig. 1. Sodium calcium silicate, crystalline phase of $Na_2Ca_2Si_3O_9$ formed the main peaks and alumina silicate in bioactive glass formed the minor phase, confirming the formation of composite BG-Al. Furthermore, a few peaks are matched with the phase of β-$Na_2Ca_4(PO_4)_2SiO_4$ of the substrate, may be owing to the formation of additional crystalline phase (Long and Rack 1998; Eliades 1997). Previous results of (Behzad and Gholam 2013) (Hanawa 1999) stated that by increasing the sintering the temperature by 850 ºC, there will be a formation of wollastonite ($CaSiO_3$) as a major phase along with sodium phosphate ($NaPO_3$). Whereas in this work at 800 ºC, the formation of sodium calcium silicate and sodium aluminum silicate phase was formed. In previous reports (Tariq et al. 2018), sodium

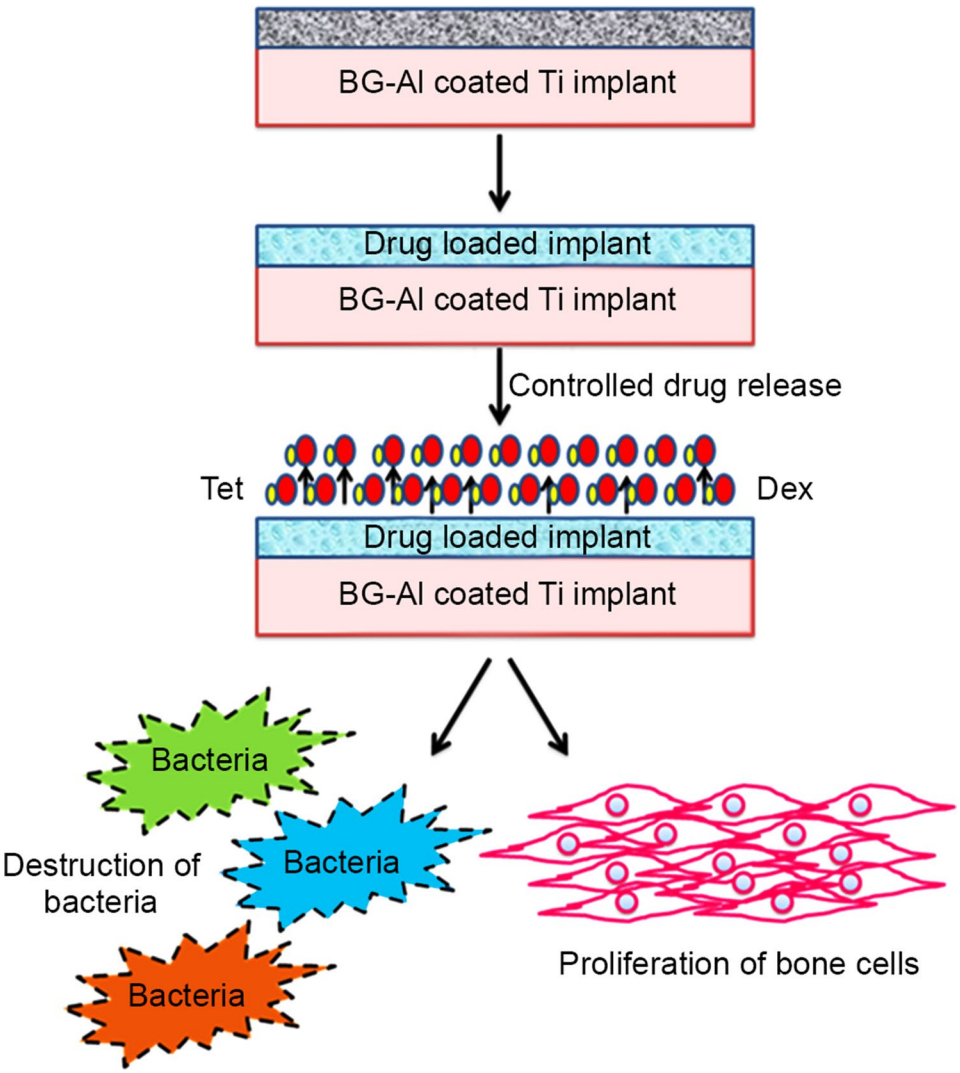

Scheme 1. A schematic illustration of dual drugs (Dexamethasone (Dex)—anti-inflammatory and Tetracycline (Tet)—antibacterial) infused Al_2O_3-bioactive glass coatings on Cp-Ti substrate that destructs the microbes and enhances the proliferation of cells for controlling orthopedic infections

calcium phosphate ($NaCaPO_4$) crystal is the primary crystal formed after sintering at 800 ℃. Crystalline phase formation is possibly due to slow nucleation on the surface and also the prompt development of nuclei. The differential grain expansion may direct to the rapid increase of silicate crystals, the residual phosphate phase migrate and surrounds the silicate crystals as a nucleating agent, and finally, it may form as $Na_2Ca_4(PO_4)_2SiO_4$ (Kaseem and Choe 2019). However, from the results of XRD, it is investigated that there was no $NaCaPO_4$ crystal phase detected, and instead, silicorhenanite (β-$Na_2Ca_4(PO_4)_2SiO_4$) and $Na_{7.15}(Al_{7.2}Si_{8.8}O_{32})$ phases were formed in the composite-coated substrate.

Those above phases were matched with JCPDF card numbers such as JCPDF (1053) and JCPDF (79–0993).

Functional group analysis

FTIR spectra of BG-Al coatings are shown as in Fig. 2. The BG spectrum shows prominent bands around 1200–850 cm^{-1} and 550–400 cm^{-1} (Behzad and Gholam 2013). Si–O-Si bending was assigned at 450 cm^{-1} and Si–O stretching at 1050 cm^{-1} and 920 cm^{-1}, respectively. The peaks become sharper and the increase in intensity of the peak is due to the increase in concentration of alumina (5%, 10%, and 15%) added to the network of BG.

Furthermore, an increase at 950–1000 cm^{-1} region is observed. The spectral samples of the substrates exhibit a band at 940 cm^{-1} which may be due to the formation of Q_{Si}^2 (Si–O–2NBO) and bands ranging at 1030 cm^{-1} and at around 490 cm^{-1} are associated with stretching and bending of Q_{Si}^3 units (Si–O–Si), respectively (Xanthappi et al. 2011; Huang et al. 2015). The main features of FTIR spectra attributing to alumina are the formation of band at around 600–850 cm^{-1} which may correspond to Si–O–Al vibrations. Additionally, the spectra of BG-Al composites, and the characteristic peaks of crystallized phases in the BG network are experimental. There are two crystalline phases recognized, such as sodium calcium silicate ($Na_2Ca_2Si_3O_9$)

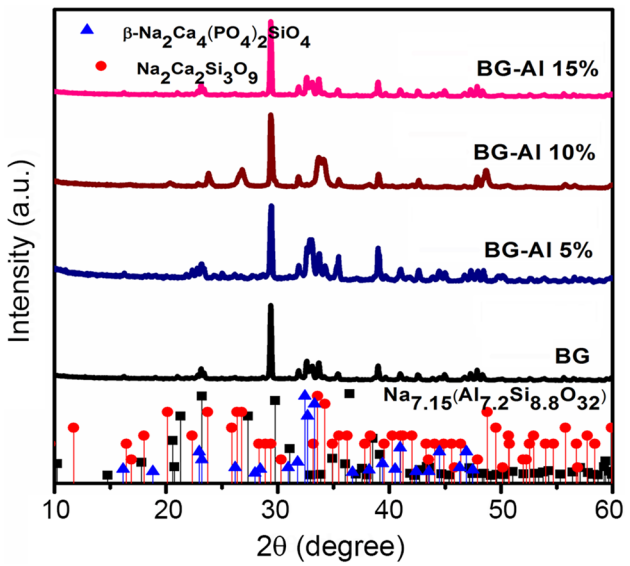

Fig. 1 X-ray diffraction patterns of BG and BG-Al composites (BG-Al 5%, BG-Al 10% and BG-Al 15%) coated Cp-Ti substrates

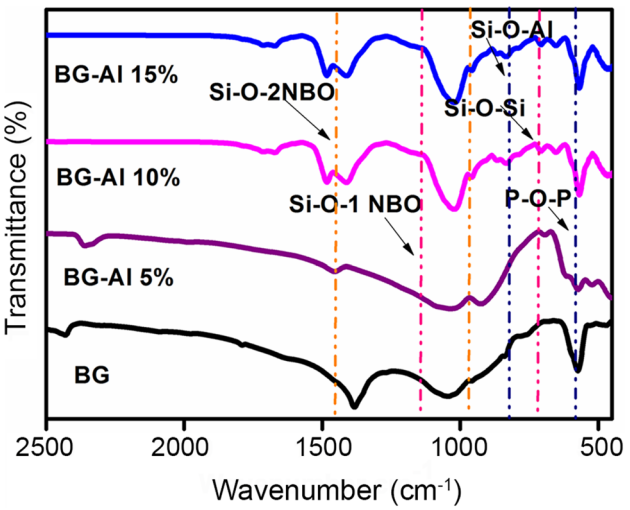

Fig. 2 FTIR spectra of BG and BG-Al composites (BG-Al 5%, BG-Al 10% and BG-Al 15%) coated Cp-Ti substrates

as major phase, and a second crystalline phase of calcium phosphate. This has been reported earlier under the same circumstances (Oslon et al. 2005; Kournetas et al. 2017). As the alumina content in the composites increases, some of the distinctive peaks of the crystalline phases of the BG such as at 575 cm^{-1}, 620 cm^{-1}, and 900 cm^{-1} are overlapped with the alumina peaks (Davies et al. 2013).

Surface morphology and surface topography study

The surface morphology of BG-Al coatings is analyzed using SEM and it is shown in Fig. 3. Non-uniform distributions of particles are observed that could be attributed to accelerated deposition that occurs with spray pyrolysis technique (Yigit et al. 2021; Kaseem and Choe 2021). Thus, deposition of particles enhanced surface roughness that facilitates higher cell adhesion and proliferation and may eventually promote osseointegration rate (Stalin et al. 2020; Oktay et al. 2021). The uniform distribution of nanoparticles is confirmed with elemental mapping method and it is shown in Fig. 4. In which elemental mapping image depicts the increase in concentration of zirconia in all three composites of BG-coated substrates.

3D surface morphology of BG and BG-Al coatings is illustrated in three dimensions in Fig. 5, as analyzed in a non-contact surface roughness tester. Central region of coatings exhibited peaks, valleys, and pits in the micro-range. Roughness in micro-scale (50 μm) is corroborated with higher Al concentration. BG-Al films presented with comb-like peak: average surface roughness was taken as R_a arithmetic mean deviation of surface roughness profile value as listed in Table 1. R_a value depicting the surface roughness clearly indicates simultaneous increase in roughness with increase in concentration of Al (metal oxide); (Hussain et al. 2020) this is an additional benefit for cell adhesion and in vitro cell proliferation (Mosab and Han-Choel 2021).

Optimal R_a value favorable for cell adhesion is observed to be 0.5–3 microns, and our findings ranged from 1.3 to 2.6 microns, which indicates improved cell adhesion facilitating enhanced osseointegration rate (Kokubo and Takadama 2006b).

Biomineralization study

Surface morphology of the biomineralized surfaces is shown in Fig. 6. The SEM micrographs of bioglass depict BG-Al 5%, BG-Al 10%, and BG-Al 15% after immersing in SBF for 1 day, 3 days, and 7 days. The BG-Al presented fine particle size in the range of 40–50 nm. Irregular sphere-like morphology of the particle aggregates were observed in pre-immersion stage. However, post-immersion, changes in topography are observed as being more protruded indicating apatite deposition (Diefenderfer et al. 2003a; Seung-Pyo et al. 2020).

The rate of apatite formation correlated with concentration of Al, and an increase in precipitation is noted with higher concentration. Apatite crystals have further exhibited flower-like and needle-like morphology with longer immersion times. Alumina has the characteristics to reduce bioactivity, but as glass formulation was done with sol/gel method, it caused formation of very small nanoparticles that

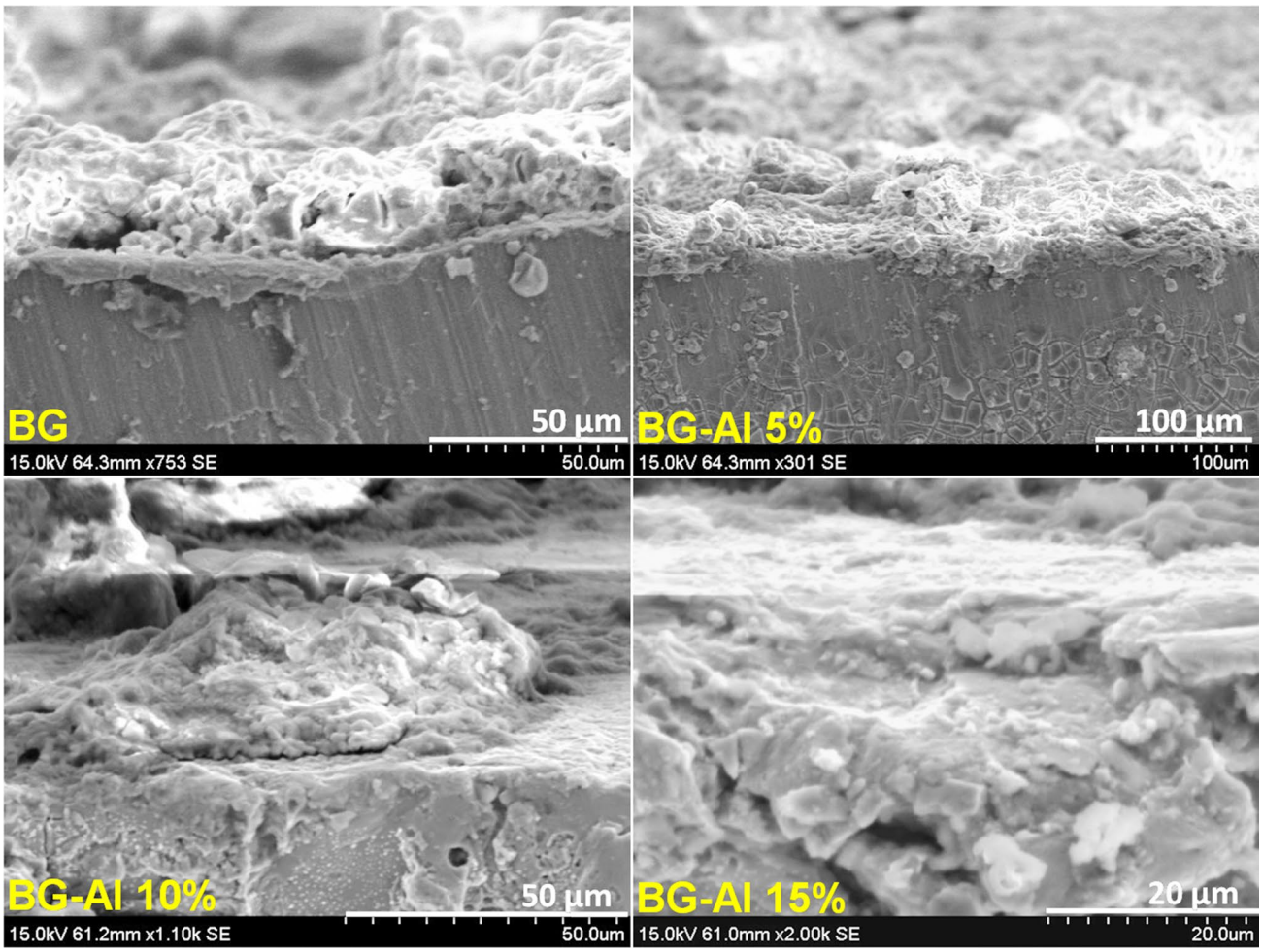

Fig. 3 Cross-sectional SEM micrographs of BG and BG-Al composites (BG-Al 5%, BG-Al 10%, and BG-Al 15%) coated Cp-Ti substrates

in turn possibly led to increase in nucleation sites (Lindberg et al. 2008), thus, prompting considerable growth of HCA layer (Mosab and Han-Choel 2019a). For BG-Al 10% and BG-Al 15% composites, bone-like apatite formation is observed as copious spherical shapes in both composites, more prominently in BG-Al 15%. This prominence is ascribed to the presence of higher Al content resulting in increase in number of Al–OH groups in Si–OH matrix culminating in augmented apatite growth. Hence, due to Al_2O_3 with high Si content, the apatite formation on the surface takes place (Diefenderfer et al. 2003b; Sollazzo et al. 2008). Presence of silanol groups is vital for HA formation as they serve as nucleation sites (Jiang et al. 2015). After initiation of nucleation, apatite growth happens spontaneously by rapid absorption of calcium phosphate ions present in surrounding fluid (Webster et al. 1999; Araujo et al. 2015).

Hemocompatibility

Hemolytic percentage of BG and BG-Al-coated Cp-Ti substrates is given in Fig. 7. ASTM standard-F756-00 (Stan et al. 2013a; Ma et al. 2010), < 2% hemolysis is considered as non-hemolytic; 2–5% is slightly hemolytic; > 5% is hemolytic. All the test samples were analyzed in triplicates, hemolytic property of BG is found to be 2.5% that is slightly hemolytic, and BG-Al 5%, BG-Al 10%, and BG-Al 15%-coated Cp-Ti substrates are non-hemolytic (displayed < 2% lysis). Considering the concentration of sample, which is in the range of 15% shows < 1.5% that is very less in toxicity and 10% shows optimal lysis. This may be due to the presence of alumina nanoparticles. Hemolytic activity of BG-Al-coated substrates clearly indicated that they are hemocompatible. Since BG-Al 10% had optimal roughness and hemocompatibility, it was chosen for further investigations.

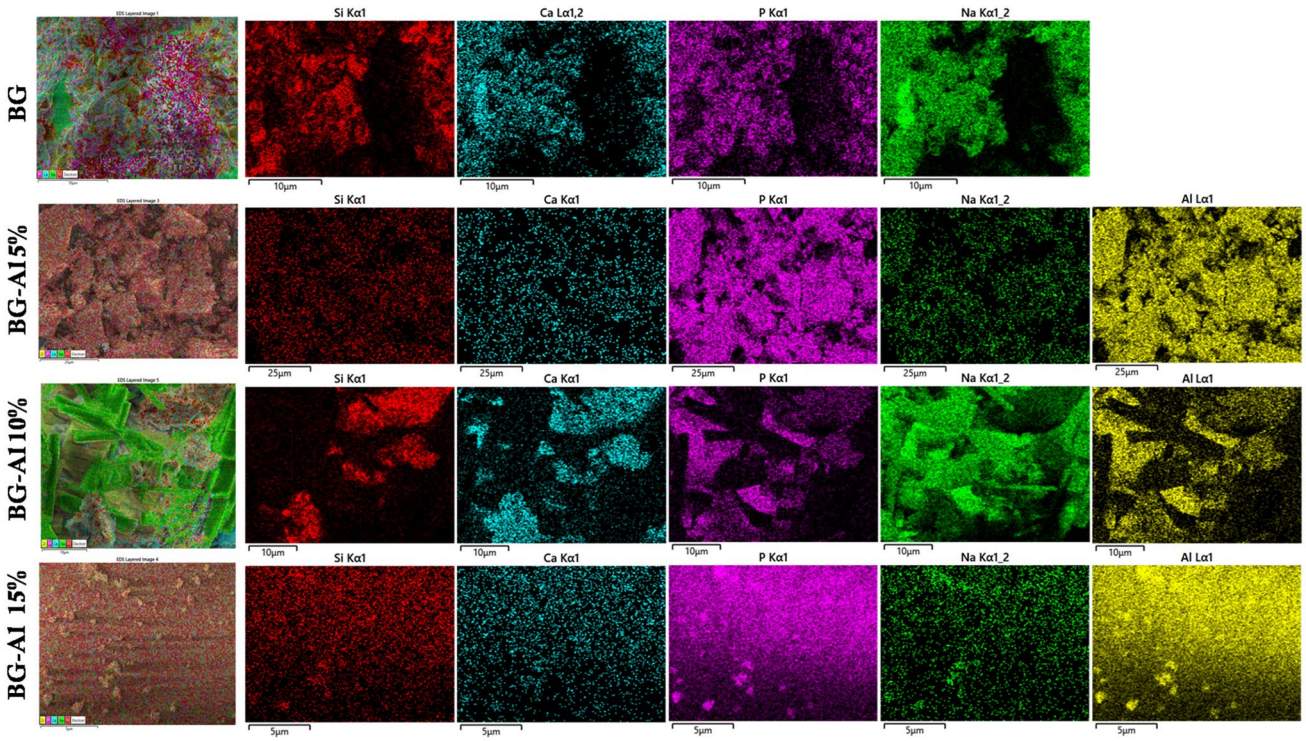

Fig. 4 Elemental mapping of BG and BG-Al composites (BG-Al 5%, BG-Al 10%, and BG-Al 15%) coated Cp-Ti substrates indicating the uniform distribution of the nanoparticles (dark red—Si, blue—Ca, purple—P, green—Na, and yellow—Al).

FTIR analysis of drug-loaded BG and BG-Al composite substrates

FTIR analysis has been carried out to confirm the presence of Dex and Tet drug-loaded BG and BG-Al-coated Cp-Ti substrates. Figure 8 indicates that the vibrational bands at 440 cm^{-1} represent Si–O–Si vibrational bending. Asymmetric vibrations of PO_4^3 is suggestive of P = O bonding at 600–550 cm^{-1}. Symmetric stretching of Si–O–Si was observed at 792 cm^{-1}. Stretching vibrations of phosphate groups appeared at 590 cm^{-1} and 604 cm^{-1} (Lin and Hwang 1996). Symmetric stretch of Si–O–Si is observed as band at 800 cm^{-1} and vibrational modes of alumina are observed at 498 cm^{-1} to 502 cm^{-1} which substantiate the presence of alumina.

Furthermore, addition of Dex loading is identified by the presence of C=O stretching vibrational peak at 1060 cm^{-1} (Wang et al. 2011). In the case of Tet drug-loaded BG and composite, as shown in Fig. 8, it is observed that there is a broadening peak at 800–900 cm^{-1} and 1100–1120 cm^{-1}. This could be implicit as a credible chemical interaction taken place between anionic groups of BG to the moiety of tetracycline acid (Ribeiro et al. 2012). Hence, it confirms the presence of Tet drug loaded in the BG system. It may be attributed to the chemical interactions that have taken place between glass anionic phosphate group and the tetracycline acid moiety (Stan et al. 2013b).

Evaluating drug release of BG and BG-Al composite substrates

To evaluate the drug-releasing efficiency, two different drugs such as Tetracycline (antibiotic) and Dexamethasone (anti-inflammatory)-loaded BG/Al coatings have been analyzed at different time intervals. The surface area and porous nature of the BG and BG-Al coatings have been used for post-implant drug-delivery applications (Depprich et al. 2008). Release profile of Tet- and Dex-loaded bioactive coatings was evaluated in PBS (pH 7.4) at room temperature. Figure 9 shows the cumulative drug release of Tet- and Dex-loaded BG and BG-Al-coated Cp-Ti substrates.

BG-loaded substrate releases comparatively low amounts of drugs compared with BG-Al-coated substrate. The BG and BG-Al composites are spray coated over the Cp-Ti substrate and the amount of drugs loaded by the substrates is very low in concentration, since the concentration of the drugs taken is 10 mg (Watanabe et al. 2012; Krajewski et al. 2005). Drugs are primarily administered through oral, intramuscular, and intravenous routes. Newer strategies for improved drug availability and distribution utilizing nano-sized biomimetic agents are constantly being tested

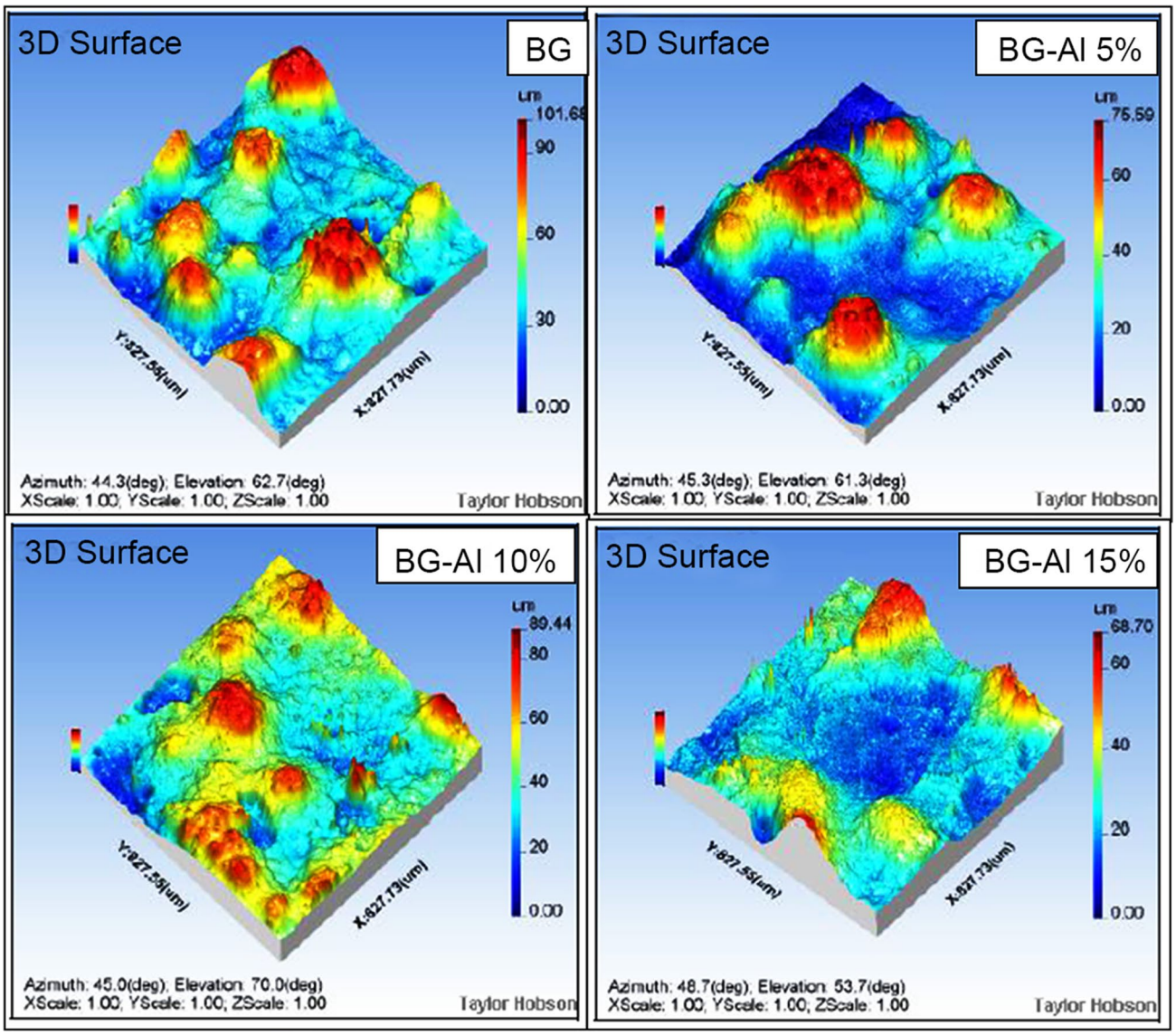

Fig. 5 3D Surface topography images of BG and BG-Al composites (BG-Al 5%, BG-Al 10%, and BG-Al 15%) coated Cp-Ti substrates

Table 1 Measurement of surface roughness on BG and BG-Al-coated substrates

Sample	R_a (μm)	R_q (μm)	R_z (μm)
BG	3.34	4.05	12.10
BG-Al 5%	1.42	1.95	9.28
BG-Al 10%	1.69	2.21	11.69
BG-Al 15%	1.87	2.22	8.34

for effective delivery at the target site (Funato et al. 2013). Nanoparticles of Alumina and BG are considered as potent drug-delivery systems due to their profound scavenging properties (Tran et al. 2013). Scavenging function is related to their antioxidant property that inhibits formation of reactive oxygen species (ROS) (Duske et al. 2015).

From these results, we can observe the slow release of drugs (Tet- and Dex-) for 6 h, and after 12 h, the amount of drug release increases in Dex- and Tet-loaded BG-Al composites than drug-loaded pure BG substrates. This may be due to reduction in porous nature and morphology of the BG bioactive materials. Basically, BGs' crystalline structure is of nanoscale and it has an inherent nanoporous structure that presents with high surface area and this unique crystalline architecture enables in biomolecules loading. Tet and Dex were studied extensively using sol/gel particles. Cavalu et al. and Zheng et al. have also reiterated the fact that surface area and porosity are key determinants in drug loading (Zheng et al. 2015a; Stoodley et al. 2011). Furthermore, drug-release

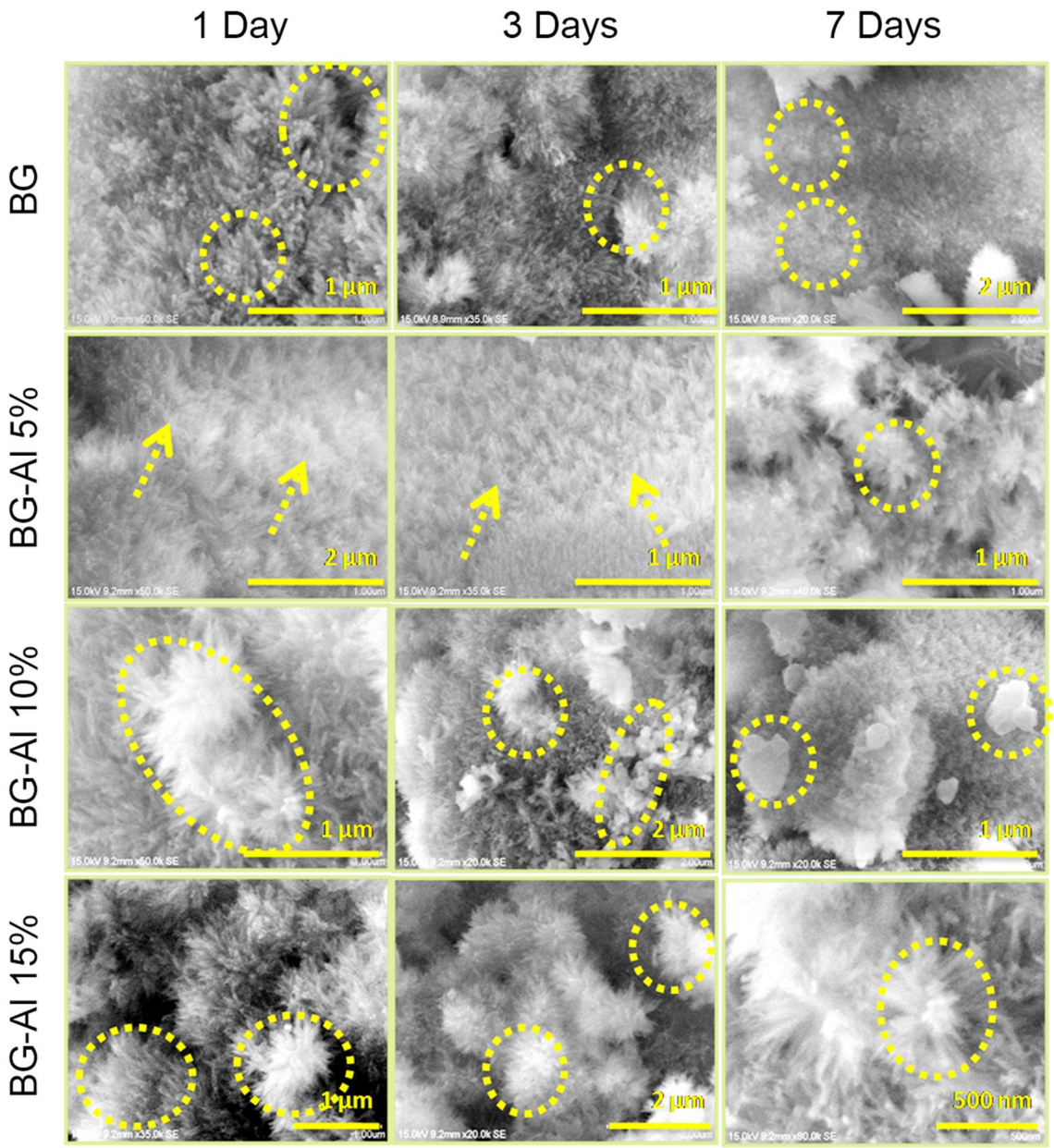

Fig. 6 SEM Surface morphological analysis of BG and BG-Al composites (BG-Al 5%, BG-Al 10%, and BG-Al 15%) coated Cp-Ti substrates after immersion in simulated body fluid at 1 day, 3 days, and 7 days

kinetics is apparently driven by diffusion through the nanoporous system. Sustained release has been enunciated; however, controlling the rate of release is a challenge yet to be overcome (Costerton et al. 1999).

In vitro cell proliferation assay

Dex-loaded BG and BG-Al nanocomposite-coated substrate shows prominent cell proliferation rate as duration increases from day 1 to day 3 than control group, as shown in Fig. 10. Optical density variation was observed with marked reduction of MTT with time and concentration (Kansal et al. 2011). Marked reduction in MTT was observed in control and BG during the 1st day of culture and further reduced during the 3rd day. MTT results revealed that there is considerable increase in number of metabolically active osteoblast-like cells. Nonetheless, the presence of 10% (% by wt) of Al in the BG matrix induces a cell proliferation compared with the control. The increase of MG-63 cell proliferation may be due to the higher percentage of alumina that has been demonstrated.

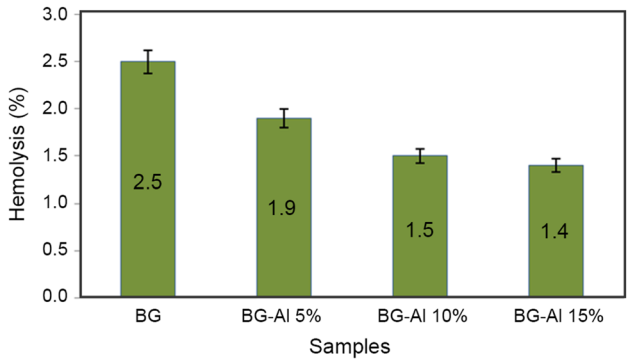

Fig. 7 Hemocompatibility analysis of BG and BG-Al composites (BG-Al 5%, BG-Al 10%, and BG-Al 15%) coated Cp-Ti substrates. Samples were analyzed in triplicate

MTT assay results clearly ascertain the biocompatible nature of BG and its nanocomposite as they support cell growth and proliferation at optimal concentration. Fast and better osseointegration is relatively stimulated through roughness of the coated substrate surface, than the proliferation rate in less rougher topographies (Somayaji et al. 2010a). Experimental evidence reveals that the cell proliferation and cell differentiation are not prominent with leveled Cp-Ti substrate layers (Mosab and Han-Choel 2019b).

However, this study substantiated that spray-coated Cp-Ti coating presented with a conductive surface for improved cell proliferation due to deposition of a coating with uniform surface roughness, predominantly contributed by aluminum oxide and Dex drug (Funato et al. 2013; Tran et al. 2013; Duske et al. 2015; Zheng et al. 2015a) (Lindberg et al. 2008; Wu et al. 2007b; Diefenderfer et al. 2003b; Osyczka et al. 2004).

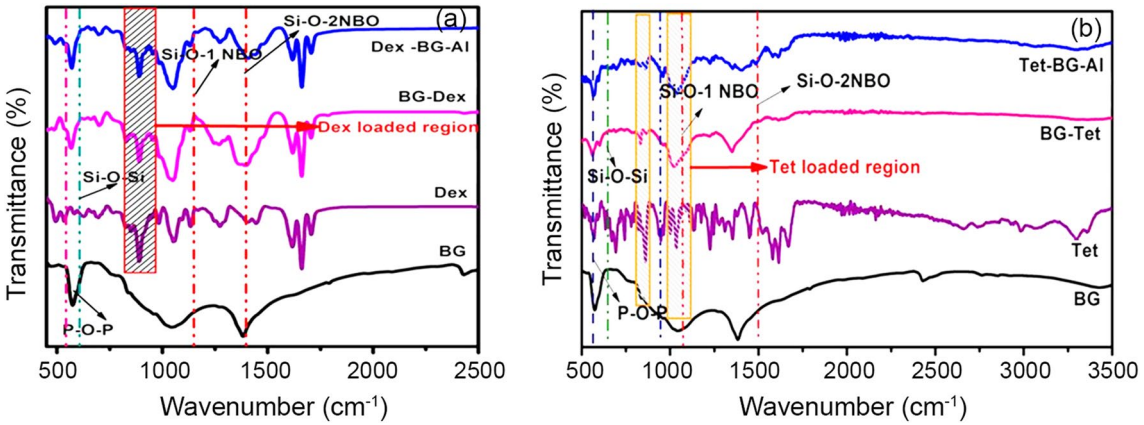

Fig. 8 FTIR spectra of (**a**) Dex and (**b**) Tet-loaded pure BG, BG-Al composite-coated Cp-Ti substrates

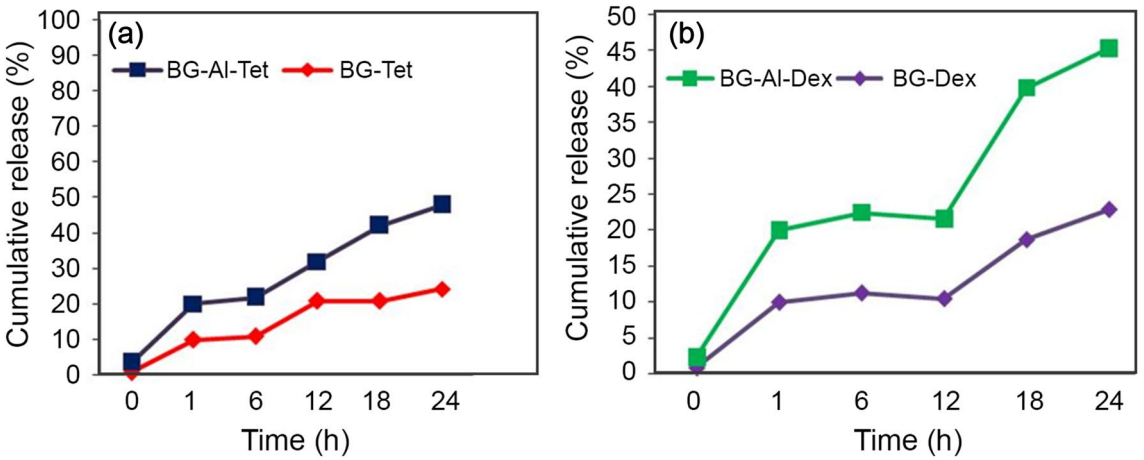

Fig. 9 Cumulative drug-release study of (**a**) Tetracycline hydrochloride (Tet) and (**b**) Dexamethasone (Dex)-loaded BG and BG-Al-coated Cp-Ti substrates

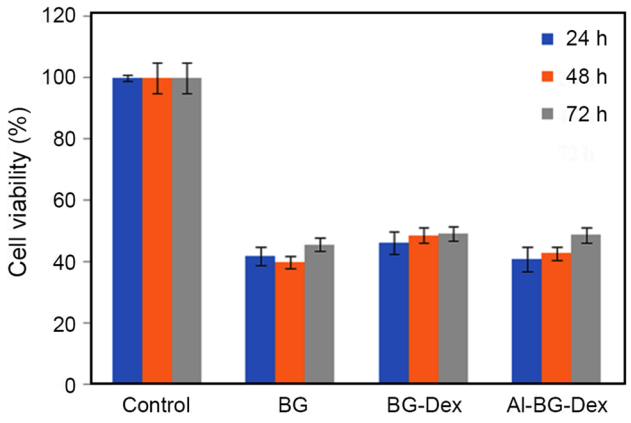

Fig. 10 In vitro cell viability rate of Dex-loaded BG and BG-Al composites (BG-Al 5%, BG-Al 10%, and BG-Al 15%) coated Cp-Ti substrates. All the samples were analyzed in triplicate

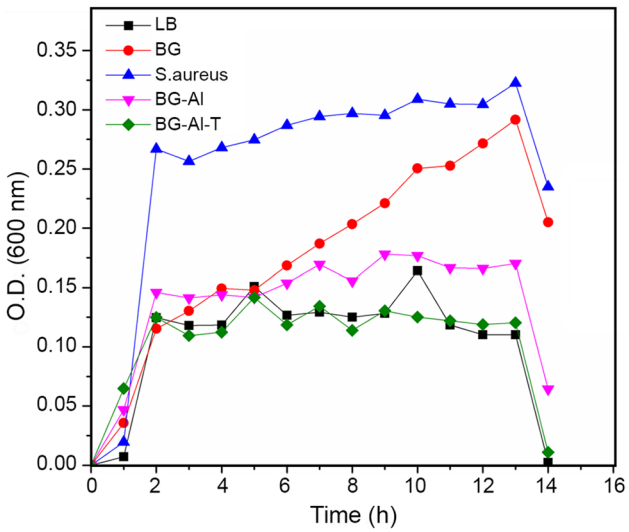

Fig. 11 Time-dependent growth inhibition assay using BG-coated and tetracycline-loaded BG-Al composite-coated Cp-Ti substrates

Remarkable osteoblast cell growth has been observed with spray-coated surface, similar outcomes in terms of osteoblast proliferation and differentiation were observed by varying the composition too (Stoodley et al. 2011; Costerton et al. 1999; Kansal et al. 2011) (Duske et al. 2015; Tran et al. 2013; Zheng et al. 2015b). Dex-loaded BG-Al exhibited pronounced ability to stimulate proliferation and differentiation than the control group (Somayaji et al. 2010a) (Stoodley et al. 2011).

Time-dependent growth inhibition assay

The growth curve of the bacterial cells treated with BG-Al, BG-Al-T, and BG coatings indicates inhibition of growth and reproduction of bacterial cells. Figure 11 shows growth curves of *S. aureus* strains, in LB broth inoculated with 10^7 CFU of bacteria-treated BG-Al, BG-Al-T, and BG coatings (Costerton and Stewart 1999; Kansal et al. 2011). It has been found that the nanocoating cause a delayed growth of the strain *S. aureus*. At significant intervals, the growth curves of *S. aureus* have been observed in three phases consisting of lag, exponential, and stabilization.

However, declined phase in each growth curve is examined and it is observed that the coatings containing Tetracycline (T)- loaded and BG-Al show negligible activity against S. aureus, which indicates that there is a control in bacterial growth. Alternatively, pure BG coatings show a rapid increase in bacterial growth and attain exponential phase, which is comparatively more or less equal with bacterial growth. Thus, in the presence of Al and Tet antibiotics, BG shows good bacterial growth inhibition than alone BG-coated substrates.

Antibacterial activity

Antibacterial activity of Tet drug-loaded pure BG and BG-Al-coated Cp-Ti substrate has been assessed with "minimal inhibitory concentration" (MIC) technique (Stoodley et al. 2011) using *P. aeruginosa*, *E. coli*, *B. subtilis*, and *S. aureus*. Results depicted in Fig. 12 ascertain inhibition of E. coli and B. subtilis, and profound inhibitory action on *P. aeruginosa* and *S. aureus*. Additionally, MIC exhibited linear advancement in the presence of alumina content, similar to earlier reports (Somayaji et al. 2010b). This attribute bestows reduced bacterial adhesion over the implant surface (Zan et al. 2010).

As reported in the literature, the results of metallic oxides can confer positive charge even in the presence of a negative charge in microorganisms (Drago et al. 2014). This eventually results in electromagnetic binding of microorganisms and metal oxides inhibiting microbial growth. Remarkable antibacterial property against Gram-negative bacteria (*E. coli*) could be attributed to the presence of positively (+) charged aluminum ions interacting with negatively (−) charged cell wall resulting in cell wall damage and cell death (Cheng et al. 2013). Furthermore, reactive oxygen species (ROS) released from alumina accumulates on cell surface and causes aggressive inhibition of *S. aureus*. Moreover, alumina causes decrease in growth rate of *E. coli* and *P. aeruginosa* by increasing membrane permeability that facilitates entry of BG-Al into membrane and cytoplasm, leading to cell death (Gao et al. 2014). Ionic dissolution of BG ultimately augments the pH and osmotic pressure unfavorable for bacterial growth over the implant surface (Mei et al. 2014). The experimental evidence of antimicrobial efficacy

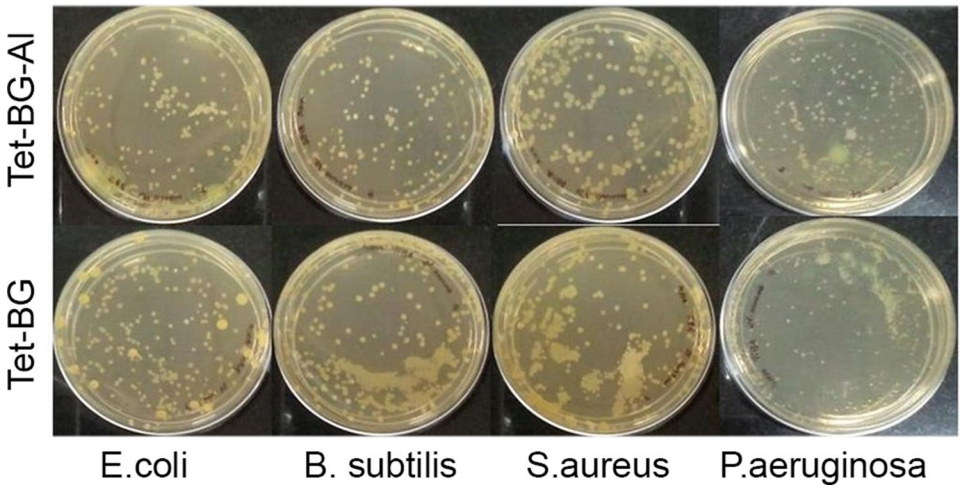

Fig. 12 Antibacterial activity of Tet-loaded BG & BG-Al-coated Cp-Ti substrates by Minimal Inhibitory Concentration

of alumina is mainly attributed to the release of metallic oxides. Jiang et al. (Dong et al. 2013) established that alumina does not cause nanoparticle-related toxicity as the ions in dissolution could not be quantified in the supernatant of the suspension. Also, it was reaffirmed that antibacterial feature of alumina nanoparticles was due to its positive charge polarizing toward the negatively charged bacterial cell wall.

Thus, pure BG coatings' result in significantly reduced colony formation against Gram-positive and Gram-negative bacteria, compared to BG-Al-coated substrates. From the above statement, it is well established that ameliorated surface roughness with substantial alumina content, along with the presence of drugs Tet in BG matrix, eventually enhances the control over biofilm accumulation. Aforementioned, bone deposition will occur unhindered in the absence of biofilm formation (Panacek et al. 2013; Kvitek et al. 2008; Knetsch and Koole 2011; Wang et al. 2013). For this reason, the drug-loaded BG and BG-Al show 10% elevated inhibitory effect on Gram-positive and Gram-negative bacteria. Thus, drug-loaded BG-Al could be a potential antibacterial coating for controlling orthopedic infections and post-implant surgical infections.

Conclusion

In this work, three different percentages by weights of Al-incorporated BG (BG-Al 5%, BG-Al 10%, and BG-Al 15%) were coated over Cp-Ti substrate using spray pyrolysis deposition. The XRD studies confirm BG-Al composite with sodium calcium aluminum silicate phase formation. Surface morphology and elemental mapping of BG-Al composites coatings showed the homogeneous distributions of nanoparticles were spray coated over the substrate. Enhanced apatite layer formation was observed, needle-like structure at day 1 to sperulites (flower)-like structure at day 7 confirms that BG-Al 15% displays higher apatite layer formation. The hemolysis results indicate that 2.5% lysis is observed in pure BG, and all BG-Al composites display less than 2% lysis. Increased cell proliferation rate was observed in BG-Al composite coatings loaded with Dex drug. The cumulative drug release of Tet- and Dex- loaded BG and BG-Al-coated substrates results indicate a gradual increase of both drugs in PBS with respect to time. This is due to the change in morphology and porous nature of the coated bioactive materials. Time-dependent growth inhibition assay results indicate negligible growth curve decline within 14 h that Tet-loaded BG-Al-coated Cp-Ti substrates than BG alone. Thus, in the presence of Al and Tet, the BG composite revealed inhibition of biofilm formation within 12 h. Hence, the surface-modified substrates coated with BG and BG-Al loaded with dual drugs such as Tet and Dex can be suggested for post-operative orthopedic implant treatment to reduction of the infections and to enhance the bone bonding ability of the implants.

Acknowledgements Authors acknowledge DBT (Department of Biotechnology) Ministry of Science and Technology, New Delhi, India. Project No: BT/PR8236/NNT/28/669 and BT/PR26836/NNT/28/1483/2017 for providing funds to execute this research work.

Declarations

Conflict of interest There are no conflicts of interest to declare.

References

Araujo M, Miola M, Bertone E, Baldi G, Perez J, Verne E (2015) On the mechanism of apatite-induced precipitation of 45S5 glass pellets coated with anatural-derived polymer. Appl Surf Sci 353:137–149

Ashok raja C, Balakumar S, Bargavi P, Rajashree P, Anandkumar B, George R P, and Kamachi Mudali U, (2018) Decoration of 1-D

Nano Bioactive Glass on Reduced Graphene Oxide Sheets: Strategies and in-vitro Bioactivity Studies. Mater. Sci. Eng. C, 90, 85-94
Behzad M, Gholam HB (2013) Crystallization behavior and microstructure of glass-ceramic system. Int Lett Chem Phys Astronomy 19:58–68
Cheng H, Li Y, Huo K, Gao B, Xiong W (2013) Long-lasting in vivo and in vitro antibacterial ability of nanostructured titania coating incorporated with silver nanoparticles. J Biomed Mater Res A 102(10):3488–3499
Clark S (2010) Surface modification of biomedical and dental implants and the processes of inflammation, wound healing and bone formation. J Mol Sci 11:354–369
Costerton JW, Stewart PS Greenberg EP (1999) Bacterial biofilms: a common cause of persistent infections. Science 284:1318-1322
Costerton JW, Stewart PS, Greenberg EP (1999) Bacterial biofilms: a common cause of persistent infections. Science 284: 1318–1322
Dalal A, Pawar V, McAllister K, Weaver C, Hallab NJ (2012) Orthopedic implant cobalt-alloy particles produce greater toxicity and inflammatory cytokines than titanium alloy and zirconium alloy based particles in-vitro, in human osteoblasts, fibroblasts, and macrophages. J Biomed Mater Res Part A 100:2147–2158
Davies JE, Ajami E, Moineddin R, Mendes VC (2013) The roles of different scale ranges of surface implant topography on the stability of the bone/implant interface. Biomaterials 34:3535–3546
Depprich R, Ommerborn M, Zipprich H, Naujoks C, Handschel J, Wiesmann HP, Norbert RK, Ulrich M (2008) Behavior of osteoblastic cells cultured on titanium and structured zirconia surfaces. Head Face Med 4:29
Diefenderfer DL, Osyczka AM, Garino JP, Leboy PS (2003a) Regulation of BMP-induced transcription in cultured human bone marrow stromal cells. J Bone Joint Surg Am 85A:19–29
Diefenderfer DL, Osyczka AM, Reilly GC, Leboy PS (2003b) BMP responsiveness in human mesenchymal stem cells. Connect Tissue Res 44(1):305–311
Dong W, Zhu Y, Zhang J, Lu L, Zhao C, Qin L, Li Y (2013) Investigation on the antibacterial micro-porous titanium with silver nanoparticles. J Nanosci Nanotechnol 13:6782–6786
Drago L, Boot W, Dimas K, Malizos K, Hansch GM, Stuyck J, Gawlitta D, Romano CL (2014) Does implant coating with antibacterial-loaded hydrogel reduce bacterial colonization and biofilm formation in vitro? Clin Orthop Relat Res.
Durgalakshmi D, Ajay Rakkesh R, Ashok Raja C, Balakumar S (2015) Electrophoretic deposition of bioglass/TiO_2 nanocomposite on CP-Ti substrates for biomedical applications. Int J Chem Tech Res 7:755–761
Durgalakshmi D, Ajay Rakkesh R, Kesavan M, Ganapathy S, Ajithkumar TG, Karthikeyan S, Balakumar S (2018) Highly reactive crystalline phase embedded strontium-bioactive Nanorods for multimodal bioactive applications. Biomater Sci 6:1764–1776
Duske K, Jablonowski L, Koban I, Matthes R, Holtfreter B, Sckell A, Nebe JB, von Woedtke T, Weltmann KD, Kocher T (2015) Cold atmospheric plasma in combination with mechanical treatment improves osteoblast growth on biofilm covered titanium discs. Biomaterials 52:327–334
Eliades T (1997) Passive film growth on titanium alloys: physicochemical and biological considerations. Int J Oral Maxillofac Implants 12:621–627
Felora H, Reza BA (2011) Synthesis and characterization of nanocrystalline zirconia powder by simple sol-gel method with glucose and fructose as organic additives. Powder Technol 205:193–200
Francesco B, Enrica V (2017) Glass-based coatings on biomedical implants: a state-of-the-art review: Biomed. Glass 3:1–17
Funato A, Yamada M, Ogawa T (2013) Success rate, healing time, and implant stability of photofunctionalized dental implants. Int J Oral Maxillofac Implants 28:1261–1271
Gao A, Hang R, Huang X, Zhao L, Zhang X, Wang L, Tang B, Ma S, Chu PK (2014) The effects of titania nanotubes with embedded silver oxide nanoparticles on bacteria and osteoblasts. Biomaterials 35:4223–4235
Geetha M, Singht AK, Asokamani R, Gogia AK (2009) Ti based biomaterials, the ultimate choice for orthopaedic implants—a review. Prog Mater Sci 54:397–425
Ghannam A, Hamazaway E, Yehia A, (2001) Effect of thermal treatment on bioactive glass microstructure, corrosion behavior, ζ potential and protein adsorption, J. Bio Med. Res., 387–395.
Gil-Albarova J, Garrido-Lahiguera R, Salinas AJ, Roman J, Bueno-Lozano AL, Gil-Albarova R, Vallet-Regi M (2004) The in vivo performance of a sol-gel glass and a glass-ceramic in the treatment of limited bone defects. Biomaterials 25:4639–4645
Guilherme A, Castilho A, Maximiliano D, Waldemar A, Macedo A (2006) Surface characterization of titanium based dental implants. Brazil J Phys 36:1004–1008
Hanawa T (1999) In-vivo metallic biomaterials and surface modification. Mater Sci Eng A 267:260–266
Hench LL, Wheeler DL, Greenspan DC (1998) Molecular control of bioactivity in sol-gel glasses. J Sol-Gel Sci Technol 13:245–250
Huang AW, Santos C, Magnago RO, Silva RFF, Strecker K, Daguano JK (2015) Sintering of alumina ceramics reinforced with a bioactive glass of $3CaO.P_2O_5$–SiO_2–MgO system. Ceramica 61:160–167
Hussain T, Kaseem M, Ko MG, (2020) Hard acid-hard base interactions responsible for densification of alumina layer for superior electrochemical performance, Corros. Sci. 170, 108663.
Indranee D, Shreyasi C, Arnab M, Biswanath K, Goutam D (2016) Fabrication of a cubic zirconia nanocoating on a titanium dental implant with excellent adhesion, hardness and biocompatibility. RSC Adv 6:59030–59038
Inuzuka M, Nakamura S, Kishi S, Yoshida K, Hashimoto K, Toda Y, Yamashita K (2004) Hydroxyapatite—doped zirconia for preparation of biomedical composites ceramics. Solid State Ion 172:509–513
Jiang P, Liang L, Song ZY, Ren L, Zhang L, Tang P, Lin C (2015) Effect of octacalcium phosphate-modified micro/nanostructured titania surfaces onosteoblast response. ACS Appl Mater Int 7:14384–14396
Kansal I, Goel A, Tulyaganov DU, Pascual MJ, Lee H, Kim HW, Ferreira JMF (2011) Diopside ($CaO_3MgO_2SiO_2$)- fluorapatite ($9CaO_3P_2O_5CaF_2$) glass-ceramics: potential materials for bone tissue engineering. J Mater Chem 21:16247–16256
Kaseem M, Choe HC (2019) Electrochemical and biochemical characteristics of the porous surface confirmed on Ti-xNb alloys via plasma electrolytic oxidation. Surf Coat Tech S0257–8972:31018–31027
Kaseem M, Choe HC (2021) Acceleration of bone formation and adhesion ability on dental implant surface via plasma electrolytic oxidation in a solution containing bone ions. Metals 11:106
Knetsch MLW, Koole LH (2011) New strategies in the development of antimicrobial coatings: the example of increasing usage of silver and silver nanoparticles. Polymers 3:340–366
Kohal RJ, Wolkewitz M, Tsakona A (2011) The effects of cyclic loading and preparation on the fracture strength of zirconium dioxide implants: an in-vitro investigation. Clin Oral Implant Res 22:808–814
Kokubo T, Takadama H (2006a) How to prepare the simulated body fluid (SBF) and its related solutions. Biomaterials 27:2907–2915
Kokubo T, Takadama H (2006b) How useful is SBF in predicting in-vivo bone bioactivity. Biomaterials 27:2907–2915
Kournetas N, Spintzyk S, Schweizer E, Sawada T, Said F, Schmid P, Geis-Gerstorfer J, Eliades G, Rupp F (2017) Comparative evaluation of topographical data of dental implant surfaces applying

optical interferometry and scanning electron microscopy. Dent Mater 2957:11

Krajewski A, Ravaglioli A, Tinti A, Taddei P, Mazzocchi M, Martinetti R, Fagnano C, Fini M (2005) Comparison between the in-vitro surface transformations of AP40 and RKKP bioactive glasses. J Mater Sci Mater Med 16:119–128

Kvitek L, Panacek A, Soukupova J, Kolar M, Vecerova R, Prucek R, Holecova M, Zboril R (2008) Effect of surfactants and polymers on stability and antibacterial activity of silver nanoparticles (NPs). J Phys Chem C 112:5825–5834

Laczka M, Cholewa-Kowalska K, Laczka-Osyczka A, Tworzydlo M, Turyna B (2000) Gel-derived materials of a $CaO–P_2O_5–SiO_2$ system modified by boron, sodium, magnesium, aluminium and fluorine compounds. J Biomed Mater Res 52:601–612

Lin S, Hwang C (1996) Structures of $CeO_2–Al_2O_3–SiO_2$ glasses. J Non-Cryst Solids 202:61–67

Lindberg F, Heinrichs J, Ericson F, Thomsen P, Engqvist H (2008) Hydroxylapatite growth on single-crystal rutile substrates. Biomaterials 29:3317–3323

Long M, Rack HJ (1998) Titanium alloys in total joint replacement—a materials science perspective. Biomaterials 19:1621–1639

Ma J, Chen CZ, Wang DG, Jiao Y, Shi JZ (2010) Effect of magnesia on the degradability and bioactivity of sol-gel derived $SiO_2–CaO–MgO–P_2O_5$ system glasses. Colloids Surf b 81:87–95

Mahwish B, Saira R, Shahzad N (2015) Structural and mechanical properties of surcose added zirconia thin films. Mater Today 2:5777–5785

Manam NS, Harun WSW, Shri DNA, Ghani SAC, Kurniwan T, Ismail MH, Ibrahim MHI (2017) Study of corrosion in biocompatible metals for implants: a review. J Alloys Compd 701:695–715

Mei S, Wang H, Wang W, Tong L, Pan H, Ruan C, Ma Q, Liu M, Yang H, Zhang L (2014) Antibacterial effects and biocompatibility of titanium surfaces with graded silver incorporation in titania nanotubes. Biomaterials 35:4255–4265

Mosab K, Han-Choel C, (2019) Triggering the hydroxyapatite deposition on the surface of PEO-coated Ti-6Al-4V alloy via the dual incorporation of Zn and Mg ions, J. Alloy. Compd, 153038.

Mosab K, Han-Choel C, (2019) Electrochemical and bioactive characteristics of the porous surface formed on Ti-xNb alloys via plasma electrolytic oxidation, Surf Coat Technol 25:125027.

Mosab K, Han-Choel C (2021) Acceleration of bone formation and adhesion ability on dental implant surface via plasma electrolytic oxidation in a solution containing bone iIons. Metals 11:106

Mosab K and Han-Chole C, (2021) The effect of in-situ reactive incorporation of MoOx on the corrosion behavior of Ti-6Al-4V alloy coated via micro-arc oxidation coating. Corr. Sci, 192, 109764.

Mosab K and Han-Chole C, (2021) Simultaneous improvement of corrosion resistance and bioactivity of a titanium alloy via wet and dry plasma treatments, J. Alloys Compd, 851, 156840.

Nayak JP, Kumar S, Bera J (2010) Sol–gel synthesis of bioglass-ceramics using rice husk ash as a source for silica and its characterization. J Non-Cryst Solids 356:1447–1451

Niedzielski K, Sindut R, Cholewa-Kowalska K, Kokoszka J, Laczka M, (2011) An in vivo study of the new generation of bioactive glass-ceramic as a substitute of bone, Eur. J. Glass Sci. Technol., A, 52, 63–66.

Oktay Y, Niyazi O, Burak D, Mosab K (2021) Surface properties of graphene functionalized TiO_2/nHA hybrid coatings made on Ti_6Al_7Nb alloys via plasma electrolytic oxidation (PEO). Molecules 26:3903

Oslon A L, Soelberg N R, Marshell D W and Anderson G L, (2005) Mineralizing, Steam reforming treatment of Hanford low activity waste, INEEl conf, 1–16.

Osyczka AM, Diefenderfer DL, Bhargave G, Leboy PS (2004) Different effects of BMP-2 on marrow stromal cells from human and rat bone. Cells Tissues Organs 176:109–119

Pamula E, Kokoszka J, Cholewa- Kowalska K, Laczka M, Kantor L, Niedzwiedzki L, Peilly GC, Filipowska J, Madej W, Kolodziejczyk M, Tylko G, Osyczka AM, (2011) Degradation, bioactivity and osteogenic potential of composites made of PLGA and two different sol-gel bioactive glasses. Biomed Eng 39:2114–2129

Pamuła E, Cholewa-Kowalska K, Szuta M, Osyczka A M, (2012) Bioactive glasses as composite components: Technological advantages and bone tissue engineering applications. In: Ramalingam M, Ramakrishna S, Best S, Biomat. Stem. Cells. Reg. Med, Boca Raton, London, New York: CRC Press Taylor & Francis Group, 239–258.

Panacek A, Balzerova A, Prucek R, Ranc V, Vecerova R, Husickova V, Pechousek J, Filip J, Zboril R, Kvitek L (2013) Preparation, characterization and antimicrobial efficiency of Ag/PDDA-diatomite nanocomposite. Colloids Surf B Biointerfaces 110:191–198

Raja CA, Balakumar S, Durgalakshmi D, George RP, Anandkumar B, Mudali UK (2016) Reduced graphene oxide/nano-bioglass composites: processing and super-anion oxide evaluation. RSC Adv 6:19657

Ribeiro M, Monteiro FJ, Ferraz MP (2012) Infection of orthopedic implants with emphasis on bacterial adhesion process and techniques used in studying bacterial-material interactions. Biomatter 2:176–194

Seung-Pyo K. Mosab K, Han-Choel C, (2020) Plasma electrolytic oxidation of Ti-25Nb-x-Ta alloys in solution containing Ca and P ions, Sur. Coat. Technol, 395, 125916.

Sollazzo V, Pezzetti F, Scarano A, Piattelli A, Bignozzi CA, Massari L, Giorgio B, Francesco C (2008) Zirconium oxide coating improves implant osseointegration in vivo. Dent Mater 24:357–361

Somayaji SN, Huet YM, Gruber HE, Hudson MC (2010a) UV-killed Staphylococcus aureus enhances adhesion and differentiation of osteoblasts on bone associated biomaterials. J Biomed Mater Res 9A:574–579

Somayaji SN, Huet YM, Gruber HE, Hudson MC (2010b) UV-killed Staphylococcus aureus enhances adhesion and differentiation of osteoblasts on bone associated biomaterials. J Biomed Mater Res 95:574–579

Stalin B, Sudha GT, Kailasanathan C, Ravichandran M, (2020) Effect of MoO3 ceramic oxide reinforcement particulates on the microstructure and corrosion behaviour of Al alloy composites processed by P/M route, Mater. Today Commun. 25, 101655.

Stan G, Popa A, Galca A, Aldica G, Ferreira F (2013a) Strong bonding between sputtered Bioglass-ceramic films and Ti-substrate implants induced by atomic inter-diffusion post-deposition heat-treatments. Appl Surf Sci 280:530–538

Stan GE, Popa AC, Galca AC, Aldica G, Ferreira JMF (2013b) Strong bonding between sputtered bioglass ceramic films and Ti-substrate implants induced by atomic inter-diffusion post-deposition heat-treatments. Appl Surf Sci 280:530–538

Stoodley P, Ehrlich GD, Sedghizadeh PP, Hall-Stoodley L, Baratz ME, Altman DT, Sotereanos NG (2011) Orthopaedic Biofilm Infections. Curr Orthop Pract 22:558–563

Tariq U, Haider Z, Chaudhary K, Hussain R and Ali J, (2018) Calcium to phosphate ratio measurements in calcium phosphates using LIBS, IOP Conf. Series: J. Phys. Conf. Ser., 1027, 012015.

Tehseen Z, Mosab K, Shakhawat H, Young Gun K (2021) Fabrication of a protective hybrid coating composed of TiO_2, MoO_2, and SiO_2 by plasma electrolytic oxidation of titanium. Metals 11:1182

Tran N, Tran PA, Jarrell J D, Engiles JB, Thomas NP, Young MD, Hayda RA, Born CT (2013) In vivo caprine model for osteomyelitis and evaluation of biofilm-resistant intramedullary nails, BioMed Res Int 674478–674489.

Verrier S, Blaker JJ, Maquet V, Hench LL, Boccaccini AR (2004) PDLLA/ Bioglass composites for soft-tissue and hard tissue engineering: an in-vitro cell biology assessment. Biomaterials 25:3013–3021

Wang M (2003) Developing bioactive composite materials for tissue replacement. Biomaterials 24:2133–2151

Wang G, Liu X, Zreiqat H, Ding C (2011) Enhanced effects of nanoscale topography on the bioactivity and osteoblast behaviors of micron rough ZrO_2 coatings. Colloids Surf B S86:267–274

Wang H, Cheng M, Hu J, Wang C, Xu S, Han CC (2013) Preparation and optimization of silver nanoparticles embedded electrospun membrane for implant associated infections prevention. ACS Appl Mater Interfaces 5:11014–11021

Watanabe H, Saito K, Kokubun K, Sasaki H, Yoshinari M (2012) Change in surface properties of zirconia and initial attachment of osteoblastlike cells with hydrophilic treatment. Dent Mater 31:806–814

Webster TJ, Siegel RW, Bizios R (1999) Osteoblast adhesion on nanophase ceramics. Biomaterials 20:1221–1227

Wheeler D L, Stokes K E, (1997) In vivo evaluation of sol-gel bioglass Part I: Histological findings. Transactions of the 23rd Annu Meet Soc Biomat, New Orleans: LA Society of Biomaterials.

Wu JM, Wang M, Osaka A (2007a) Bioactive composite coating on titanium implants for hard tissue repair, Key Eng. Mater 334–335:1249–1252

Wu C, Ramaswamy Y, Soeparto A, Zreiqat H (2007b) Incorporation of titanium into calcium silicate improved theirs chemical stability and biological properties. J Biomed Mater Res A 86:402–410

Xanthappi C, Nikolaos K, Eleana K, Boccacini AR, Konstantinoas NP (2011) Thermal analysis and in-vitro bioactivity of bioactive glass-alumina composites. Mat Charecter 62:118–129

Xie YT, Liu XY, Ding CX, Chu PK (2005) Bioconductivity and mechanical properties of Plasma—sprayed dicalcium silicate/zirconia composite coating. Mater Sci Eng C 25:509–515

Yigit O, Ozdemir N, Dikici B, Kaseem M (2021) Surface properties of graphene functionalized TiO2/nHA hybrid coatings made on Ti6Al7Nb alloys via plasma electrolytic oxidation (PEO). Molecules 26(13):3903

Zan X, Kozlov M, McCarthy TJ, Su Z (2010) Covalently attached, silver-doped poly(vinyl alcohol) hydrogel films on poly(L-lactic acid). Biomacromol 11:1082–1088

Zheng M, Yang Y, Liu XQ, Liu MY, Zhang XF, Wang X, Li HP, Tan JG (2015) Enhanced biological behavior of in-vitro human gingival fFibroblasts on cold plasma-treated zirconia, PloS One 10: e0140278.

Zheng M, Yang Y, Liu XQ, Liu MY, Zhang XF, Wang X, Li HP, Tan JG (2015) Enhanced biological behavior of in-vitro human gingival fibroblasts on cold plasma-treated zirconia, PloS One 10: e0140278.

Publisher's Note Springer Nature remains neutral with regard to jurisdictional claims in published maps and institutional affiliations.